Chemosphere 176 (2017) 273–287

Contents lists available at ScienceDirect

Chemosphere

journal homepage: www.elsevier.com/locate/chemosphere

Prominent features in isotopic, chemical and dust stratigraphies from coastal East Antarctic ice sheet (Eastern Wilkes Land)

L. Caiazzo [a], G. Baccolo [b, c], C. Barbante [d, e], S. Becagli [a, *], M. Bertò [e], V. Ciardini [f], I. Crotti [b], B. Delmonte [b], G. Dreossi [e], M. Frezzotti [f], J. Gabrieli [e], F. Giardi [a], Y. Han [g], S.-B. Hong [g], S.D. Hur [g], H. Hwang [g], J.-H. Kang [g], B. Narcisi [f], M. Proposito [f], C. Scarchilli [f], E. Selmo [h], M. Severi [a], A. Spolaor [d, e], B. Stenni [e], R. Traversi [a], R. Udisti [a, i]

[a] Dept. of Chemistry "Ugo Schiff", University of Florence, Via della Lastruccia, 3, 50019 Sesto F.no (Florence), Italy
[b] DISAT-University Milano-Bicocca, Piazza della Scienza, 1, 20126 Milano, Italy
[c] University of Siena, Earth Science Department, Via Laterino, 8, 53100 Siena, Italy
[d] Institute for the Dynamics of Environmental Processes-CNR, Via Torino, 155, 30172 Venice-Mestre, Italy
[e] DAIS, Ca' Foscari University of Venice, Via Torino, 155, Venice-Mestre, Italy
[f] Laboratory for Earth Observations and Analyses, ENEA - C.R. Casaccia, I-00123 Rome, Italy
[g] Korea Polar Research Institute (KOPRI), 26 Songdomirearo, Yeonsu-gu, Incheon 21990, Republic of Korea
[h] Department of Chemistry, Life Sciences and Environmental Sustainability, University of Parma, Parco Area delle Scienze, 11/A, Parma, Italy
[i] ISAC CNR, Via Gobetti 101, 40129, Bologna, Italy

HIGHLIGHTS

- Ions, MSA, I, Br, BC and dust record from coastal East Antarctica are presented.
- Seasonal pattern of each markers is highlighted by comparison with $\delta^{18}O$.
- $NssSO_4^{2-}$ and $\delta^{18}O$ are chosen for annual layer counting.
- The mean accumulation rate over the period 2008–2013 is 242 ± 71 mm w.e..
- Nitrate and MSA appear to be well preserved in this high accumulation rate site.

GRAPHICAL ABSTRACT

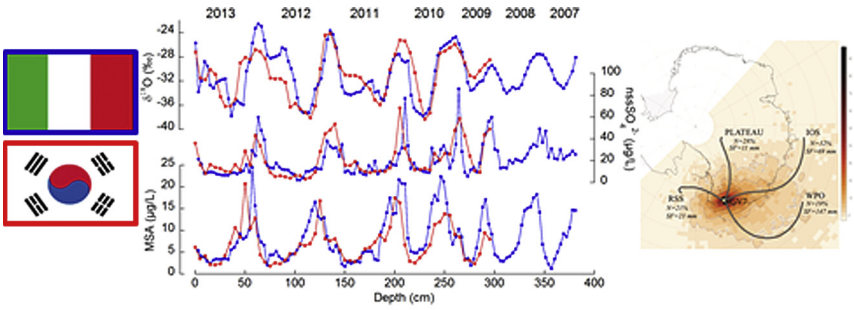

ARTICLE INFO

Article history:
Received 10 October 2016
Received in revised form
17 February 2017
Accepted 22 February 2017

Handling Editor: J. de Boer

Keywords:
Chemical composition
Snow pit

ABSTRACT

In this work we present the isotopic, chemical and dust stratigraphies of two snow pits sampled in 2013/14 at GV7 (coastal East Antarctica: 70°41′ S - 158°51′ E, 1950 m a.s.l.). A large number of chemical species are measured aiming to study their potentiality as environmental changes markers. Seasonal cluster backward trajectories analysis was performed and compared with chemical marker stratigraphies.

Sea spray aerosol is delivered to the sampling site together with snow precipitation especially in autumn-winter by air masses arising from Western Pacific Ocean sector.

Dust show maximum concentration in spring when the air masses arising from Ross Sea sector mobilize mineral dust from ice-free areas of the Transantarctic mountains.

The clear seasonal pattern of sulfur oxidized compounds allows the dating of the snow-pit and the calculation of the mean accumulation rate, which is 242 ± 71 mm w.e. for the period 2008–2013.

* Corresponding author.
E-mail address: silvia.becagli@unifi.it (S. Becagli).

http://dx.doi.org/10.1016/j.chemosphere.2017.02.115

East Antarctica
Dating
Seasonal pattern
GV7

Methanesulfonic acid and NO_3^- do not show any concentration decreasing trend as depth increases, also considering a 12 m firn core record. Therefore these two compounds are not affected by post-depositional processes at this site and can be considered reliable markers for past environmental changes reconstruction.

The rBC snow-pit record shows the highest values in summer 2012 likely related to large biomass burning even occurred in Australia in this summer.

The undisturbed accumulation rate for this site is demonstrated by the agreement between the chemical stratigraphies and the annual accumulation rate of the two snow-pits analysed in Italian and Korean laboratories.

1. Introduction

The Antarctic ice sheet and the surrounding ocean play a key role in climate dynamics (e.g. EPICA comm. Members, 2006). Causes and control factors of the current climate change are not yet fully understood (IPCC, 2013); for these reasons, increasing attention has been recently paid to natural climate variability over the last millennium, as compared to anthropogenic climate forcing occurred during the last century (Stenni et al., 2002).

Several research and study have been extensively carried out all over the Antarctic ice-sheet, with different spatial and temporal resolutions and coverages (e.g. Wolff et al., 2010; Abram et al., 2013; Delmonte et al., 2002; Traversi et al., 2012). However, due to the complexity of climate, to the vastness and variability of Antarctic ice-sheet (e.g. high spatial variability of recent temperature trend within Antarctica) and to spatial and temporal lack of instrumental and satellite data (covering only the last 30–50 years), further work is still necessary. In particular, additional ice cores are needed to achieve an adequate length of the climate record and sufficient temporal resolution to be incorporated into continental-scale climate reconstructions and model simulations.

Deep ice cores drilled in central Antarctica provide unique information on the past climate variability spanning up to the last 800 kyr (Wolff et al., 2010; Fischer et al., 2007; Watanabe et al., 1999); conversely, climate variability of the last decades remains poorly documented and understood. This is particularly the case for coastal Antarctic areas, which play a key role for the overall Antarctic mass balance (Agosta et al., 2013; Palerme et al., 2016), with relevance for global sea level (Church et al., 2013). Finally, field data are needed to assess the validity of climate models for multi-decadal variability and change in coastal Antarctic temperature and mass balance (Krinner et al., 2007).

This work is focused on Northern Victoria Land and Eastern Wilkes Land (East Antarctica) sector, where GV7 site (70°41′17.1″ S, 158°51′48.9″) is located. GV7 is situated on north–south transect following the ice divide extending from the Oates Coast to Talos Dome.

The GV7 drilling was accomplished through a bilateral Italy – South Korea collaboration, during the 2013/2014 Antarctic summer field. Snow pit samples, shallow firn cores and a 250 m deep ice core were collected and subsequently analysed, in order to study chemical species, isotopes, mineral dust and tephra, so as to produce a stacked firn/ice core record.

GV7 is located in an accumulation area which has been proposed as a potential site for achieving a continuous, high-resolution ice core record of climate and environmental variability in East Antarctica along the last millennium, with a time resolution comparable to meteorological measurements (Becagli et al., 2004; Genoni et al., 2008; Proposito and Frezzotti, 2008).

In this work we present an extensive chemical data set, covering 7 years of deposition, upon the analysis of a large number of chemical species.

Among the analysed species we report here δ^2H e $\delta^{18}O$ as site temperature proxy (e.g. Stenni et al., 2016); deuterium excess for the relative humidity at the moisture source area (e.g. Pfahl and Sodemann, 2014); Na^+, Cl^- and Mg^{2+} as marker of sea spray (e.g. Benassai et al., 2005); dust and non-sea salt Ca^{2+} ($nssCa^{2+}$) as tracer of crustal input; methanesulfonic acid (MSA) and $nssSO_4^{2-}$ for biogenic activity in the surrounding ocean (Becagli et al., 2012); NO_3^- as a marker of stratosphere/troposphere interchanges, lightning and other photo-induced atmospheric processes (e.g. Traversi et al., 2012 and 2014); I and Br enrichment as marker of sea ice extent (Spolaor et al., 2014) and refractory black carbon as marker of biomass burning (e.g. Bisiaux et al., 2012).

The chemical data set is compared with stable isotope composition and backward trajectories analysis in order to highlight and interpret the seasonal pattern of each marker. The aim of this study is to perform a survey of the GV7 site focusing on the obtainment of the following information:

- assessment of reliability of the temporal records from GV7 of species that exhibit a not complete preservation in low accumulation sites as NO_3^- and MSA;
- evaluation of the markers seasonality with specific attention to the markers (iodine and bromine enrichment and refractory black carbon) which are not commonly measured in Antarctic snow due to their very low concentration and the need of specific analytical equipment. Preliminary assessment of their possible use as marker of source intensity and transport processes in this site,
- check of the presence of undisturbed stratigraphies by the analysis of two snow pits drilled 10 m apart from each other,
- quantification of the mean accumulation rate at the site and its temporal trend also in comparison with previous data from the same site.

2. Methods

2.1. Sampling site

GV7 (70°41′17.1″ S, 158°51′48.9″ E; 1950 m a.s.l.) is located on the ice divide extending from the Oates Coast to Talos Dome, about 95 km from the Southern Ocean coast and 200 km from Talos Dome (Fig. 1). The firn temperature at 30 m depth, representing the annual average at the site, is T = −31.8 °C (Frezzotti et al., 2007).

This site was firstly investigated during the 2001/2002 ITASE traverse, where a 55 m deep firn core was retrieved. Mean snow accumulation rate reported in this occasion was 241 ± 13 mm we yr^{-1} over the past 50 years (Magand et al., 2004; Frezzotti et al.,

2007). It was calculated using the 1965–1966 radioactive horizon associated to nuclear bomb tests revealed by tritium activity (Stenni et al., 2002; Magand et al., 2004; Frezzotti et al., 2007). Besides the high accumulation rate, one of the highest observed during the 2001/2002 ITASE traverse, this site is characterized by an ice thickness of about 1700 m (Magand et al., 2004; Frezzotti et al., 2007), which could allow to obtain a very high-resolution records for the last 1–2 kyr. Besides, because of the low ratio between noise and accumulation a very well time resolved and preserved geochemical and paleoclimate records will be achieved.

Satellite images, studies of slopes, surface conditions and wind direction data, show that this site is in a flat area where katabatic winds don't have a deep influence on local re-distribution of deposited snow and on post-depositional processes (Magand et al., 2004; Frezzotti et al., 2007).

Indeed, analyses of snow radar and GPS data upstream GV7 show that internal layering and surface elevation are continuous and horizontal up to 10 km from the site, revealing low ice velocity (0.30 ± 0.01 m yr^{-1}), absence of isochrones distortions due to ice flow dynamics and very low snow accumulation spatial variability (less than 5%) (Frezzotti et al., 2007).

A preliminary age/depth model based on the accumulation rate and snow density roughly predicts that the upper 500 m (~30% of the total ice thickness) cover more than 2 kyr, with a resolution of ~2 yr m^{-1} at surface, ~4 yr m-^{1} at 50 m and ~6 yr m^{-1} at 500 m depth.

2.2. Snow pit and firn core sampling

On December 2013 two snow pits were dug by a snow cat at GV7 at a distance of about 10 m from each other. One was devoted to the Italian group, the second one to the Korean group.

As the dominant wind direction at the GV7 site is from south, the selected sampling site for the snow pits dug was approximately 250 m south of the GV7 camp to minimize the influence of human activities. The sampling and handling operation were performed following clean protocols and great precautions were taken during all the steps of all laboratory and field activities including bottle preparation, sample collection, handling, and storage to prevent sample contamination (Udisti et al., 1998 and references therein). During the field campaign, all personnel wore full cleanroom suits, polyethylene gloves, and particle masks.

The Italian snow pit (hereafter IT-SP) was 384 cm deep, and 127 samples were collected continuously along 3 parallel vertical lines on the wall of the snow pit after cleaning the wall of the pit by removing 50 cm of snow by a plastic scraper. Samples were collected in pre-cleaned (by 3 time washing with ultrapure water; resistivity > 18 MΩ) PET containers. The mean resolution was 3 cm for ions, dust and isotopic composition determination. Samples for halogen analysis were also collected in the same snow pit with a 5 cm resolution to a depth of 250 cm.

The Korean snow pit (hereafter ROK-SP) was 300 cm deep; samples were collected after removing the snow from the wall of

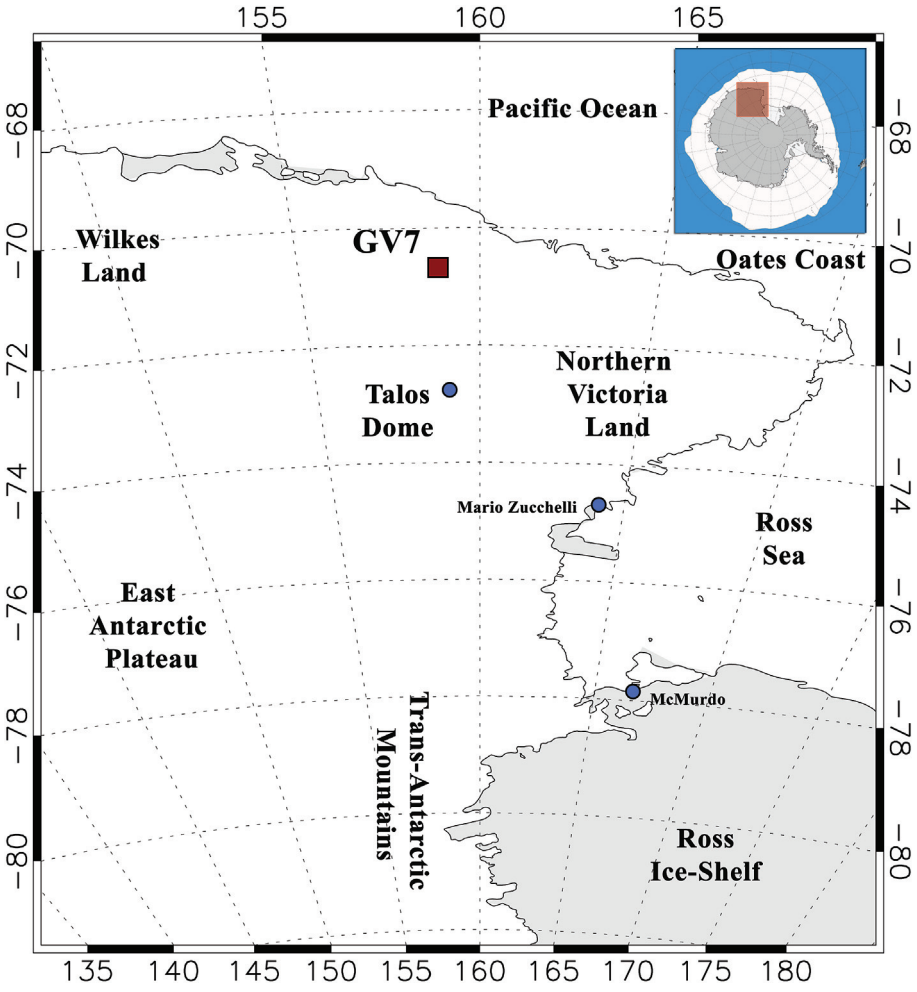

Fig. 1. Map of the Antarctica with the GV7 site.

the pit using pre-cleaned LDPE shovels. 60 snow samples were collected with a pre-cleaned PTFE tube and a hammer (mean resolution of 5 cm). Snow samples were transferred into pre-cleaned 1 L LDPE bottles.

All the containers were labelled and stored in sealed polyethylene bags, transported to Italian and Korean laboratories, where they were stored in −20 °C cold rooms until analysis.

A 12 m firn core (GV7D) was drilled starting from the surface in the same Antarctic campaign. The drilling site was located approximately 200 m south from the snow pits area and the 12 m cores have been recovered using an aluminium drill with internal diameter of 100 mm. The drilling system was equipped with solar paned and no drilling fluid were used.

Measurements of density were performed during sampling; they point to an average density of 0.42 g cm^{-3} for the first 3 m.

Field observations revealed that summer melt layers were not present at depth in any of the snow pits.

2.3. Chemical analysis

Analyses of the samples were carried out in Italy and in Korea following the procedures reported below.

2.3.1. Measurements performed in Italy

Ionic measurements were carried out at University of Florence, using DX 500 and ICS1000 Thermo-Fisher Dionex conductivity-suppressed chromatography in an integrated system. This system allows the simultaneous determination of anions (F^-, Formate, MSA, Cl^-, NO_3^-, SO_4^{2-}) and cations (Na^+, NH_4^+, K^+, Mg^{2+}, Ca^{2+}). Anion or cation detection limits ranged from 0.01 to 0.15 μg L^{-1}. The detailed description of the ions determination and performances is reported in Caiazzo et al. (2016) and Morganti et al. (2007).

Stable isotope ($\delta^{18}O$, δ^2H) measurements were carried out at the Ca' Foscari University of Venice. Each sample was preserved frozen (−20 °C) in a sealed air-tight plastic bag. In Italy the samples were melted at room temperature (≈+20 °C) and transferred into HDPE (high density polyethylene) 25 ml Kartell bottles then immediately stored in freezers (≈-20 °C) until the they were analysed. In this way any alteration of the isotopic composition due to the contact of the samples with the air lab is avoided. The samples were analysed by means of Isotopic Ratio Mass Spectrometry (IRMS), using a Thermo-Fisher Delta Plus Advantage mass spectrometer coupled with an automatic equilibration device (HDO device®) for sample injection in the mass spectrometer. The analytical method is characterized by an analytical precision of ±0.05‰ (1 σ) for $\delta^{18}O$, ±0.7‰ (1 σ) for δ^2H. With these $\delta^{18}O$ and δ^2H analytical precision, the deuterium excess was then calculated with a final precision of ±0.8‰ (1 σ). All the sample analyses have been calibrated against internal isotopic standards which are calibrated against IAEA isotopic standards every two years.

Dust concentration and size distribution measurements have been performed at EuroCold Laboratory (DISAT, University Milano-Bicocca) using Beckman Coulter Multisizer IV particle counter and a 30 μm orifice allowing detection of micro particles from 600 nm to about 18 μm. The procedure adopted in this study is similar to Delmonte et al. (2002). Total particles refer to measurements performed immediately after sample melting, insoluble particles refer to measurements performed 24 h after sample melting, following Sala et al. (2008).

Concentrations of Br, I and Na are determined at the DAIS of the Ca' Foscari University of Venice by Inductively Coupled Plasma Sector Field Mass Spectrometry (ICP-SFMS; Element2, Thermo-Fischer, Bremen, Germany) equipped with a cyclonic Peltier-cooled spray chamber (ESI, Omaha, USA). Prior to each analysis session the analytical system was cleaned for 24 h by alternating 180 s washes of 2% HNO_3 acid (trace metal grade, Romil, UK), then 180 s of ultrapure water (resistivity > 18 MΩ). Between each analysis a single cleaning cycle was run to return the background to within 1% of the initial background level (Spolaor et al., 2016).

Concentrations of refractory black carbon (rBC) were determined at the DAIS of the Ca' Foscari University of Venice by using a single-particle soot photometer (SP2) manufactured by Droplet Measurement Technologies (Boulder, CO, USA). A complete description of the SP2 functioning and physical principles are given by Stephens et al. (2003), Schwarz et al. (2006), Moteki and Kondo (2010) and Petzold et al. (2013).

The liquid samples were nebulized by means of an APEX-Q system (EPOND, Switzerland) and the nebulization efficiency was determined prior to each analytical session by using solutions of ultra-fine graphite (Aquadag®, Acheson Inc., USA) at different concentrations in ultra-pure water (Lim et al., 2014); the rBC concentrations were corrected for the nebulization efficiency by applying a factor of 0.56 (Lim et al., 2014; Kaspari et al., 2014). The samples underwent a melting/refreezing cycle before being melted and analysed, leading to a rBC loss of 38 ± 16% (Lim et al., 2014); consequently, a second correction factor was applied to the rBC concentration values. For each sample, the rBC concentration was obtained by summing the masses of particles characterized by a mass equivalent diameter in the range from 50 to 600 nm. The reported rBC concentration values are characterized by an estimated instrumental uncertainty of 20%.

2.3.2. Measurements performed in Korea

Stable water isotopes ratios were determined using a wavelength-scanned cavity ring-down spectrometer (L2140-i, Picarro Inc., USA) at KOPRI. Each sample was filtered using a 0.45 mm PVDF syringe filter (Merck Millipore, USA) and filled in a 2 mL glass vial. All plastic and glass wares were dried for more than 24 h at 80 °C before use. Vienna Standard Mean Ocean Water (VSMOW2), Greenland Ice Sheet Precipitation (GISP), and Standard Light Antarctic Precipitation (SLAP2) were used to calibrate the analyzer. To check instrumental drift, an in-house standard solution made of Antarctic snowmelt was measured every five samples. The long-term reproducibility for $\delta^{18}O$ and δ^2H were 0.05 and 0.4‰, respectively (Kang et al., 2015).

All anion and cation species have been analysed at KOPRI using a two-channel IC system combining two Dionex IC sets (ICS-2000 and ICS-2100; Thermo Fisher Scientific Inc., USA). This system makes it possible to simultaneously determine both anions and cations with reduced sample volume (~3 mL) and analysis time of ~25 min. Anions have been measured using a Dionex model ICS-2000 with an IonPac AS15 column and KOH eluent (6–55 mM). Cations have been measured using a Dionex model ICS-2100 with an IonPac CS12A column and MSA eluent (20 mM). Detection limits of major ions are calculated as the concentration corresponding to three times the standard deviation of blank measurements. The detection limits for the measured ions ranged from 0.01 to 0.26 ng mL^{-1} (Hong et al., 2015).

The analytical procedure for dust concentration and size distribution was adopted from previous studies with minor modifications (Delmonte et al., 2002; Kang et al., 2015). The measurements of dust concentration and size distribution were performed using a Multisizer 4e Coulter Counter (Beckmann Coulter, USA) with a 30 μm diameter aperture tube in a Class 100 clean booth. The melted snow sample was made conductive by the addition of a pre-filtered 20% NaCl solution to obtain a 2% electrolyte solution. The samples were continuously stirred before analysis to avoid dust sedimentation in the Accuvette cups. Three consecutive measurements were performed on each 500 μL volume. The Coulter Counter was calibrated using a Coulter CC Size

Standard L3 (Beckmann Coulter, USA) with nominal 3.0 μm diameter polystyrene latex beads. The instrument was set for measurements of particles with diameters between 0.6 and 18.0 μm in 400 channels on a logarithmic size scale. Particle size is expressed by the diameter of a sphere of equivalent volume and particle mass was calculated from the measured volume assuming a mean crustal particle density of 2.5 g cm^{-3}.

2.4. Second order parameter calculation

The Deuterium excess (d) is defined by the equation $d = 8^{*}\delta^{18}O\text{-}\delta^{2}H$ (Dansgaard, 1964), derived by the global meteoric water line: $\delta^{2}H = 8^{*}\delta^{18}O+10$ (Craig, 1961), in which the global mean d is equal to 10.

In order to evaluate quantitatively the contribution of the crustal source to Na^{+}, the sea-salt fraction of Na^{+} ($ssNa^{+}$) is calculated by using the Ca^{2+} total concentration ($totCa^{2+}$) by using the following two-equation system:

$$ssNa^{+} = totNa^{+} - nssCa^{2+} * \left(Na^{+}/Ca^{2+}\right)_{crust}$$

$$nssCa^{2+} = totCa^{2+} - ssNa^{+} * \left(Ca^{2+}/Na^{+}\right)_{sw}$$

where $(Ca^{2+}/Na^{+})_{sw} = 0.038$ represents the mean Ca^{2+}/Na^{+} ratio (w/w) in bulk seawater (Bowen, 1979) and $(Na^{+}/Ca^{2+})_{crust} = 0.56$ the mean Na^{+}/Ca^{2+} ratio in the Earth's crust (Bowen, 1979).

The fraction of sulfate arising from gaseous compounds oxidative reactions in the atmosphere (non-sea salt sulfate, $nssSO_4^{2-}$) is calculated using $ssNa^{+}$ as sea-spray marker, according to the equation:

$$nssSO_4^{2-} = totSO_4^{2-} - \left(SO_4^{2-}/Na^{+}\right)_{sw} * ssNa^{+}$$

where the $(SO_4^{2-}/Na^{+})_{sw}$ is 0.25 and represents the mean theoretical ratio (w/w) in sea water (Henderson and Henderson, 2009).

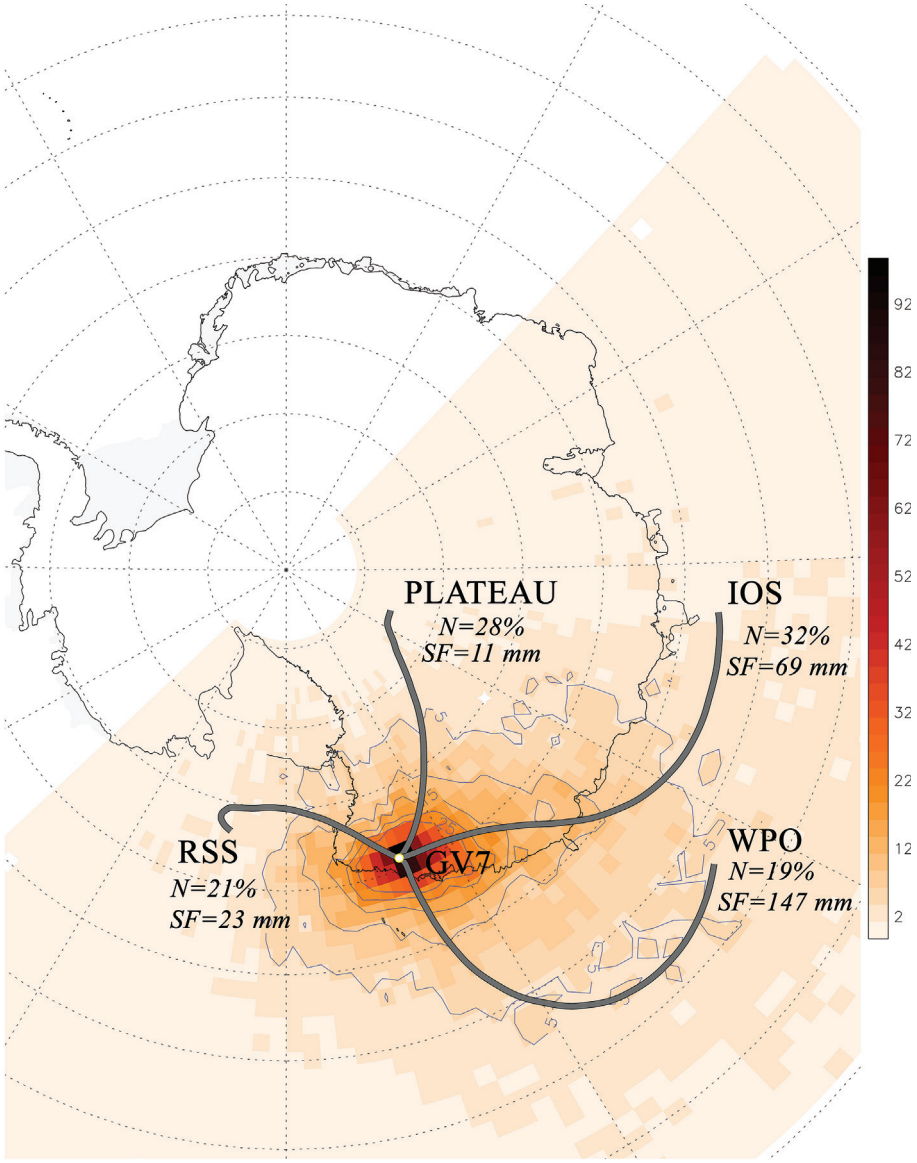

Fig. 2. Percentage of number of TJ points (i.e. number of hours) for each area of 2° × 1° (filled polygons). Contour in blue represents values up to 30%. The means TJs (in dark grey) representative of the four clusters (PLATEAU, Western Pacific Ocean-WPO, Indian Ocean - IO and Ross Sea Sector - RSS) obtained applying the k-means clustering are superimposed.

The bromine and iodine enrichment (hereafter Br_{enr} and I_{enr}) are calculated as following:

$$Br_{enr} = (Br/Na)/(Br/Na)_{sw}$$

$$I_{enr} = (I/Na)/(I/Na)_{sw}$$

where Br, I and Na are the concentration in the sample measured by ICP-SFMS and $(Br/Na)_{sw}$ and $(I/Na)_{sw}$ are the averaged mass ratio in seawater and fresh sea spray. $(Br/Na)_{sw}$ is 0.006 w/w and $(I/Na)_{sw}$ is $5.71*10^{-6}$ w/w (Millero, 1974).

2.5. Back trajectories calculation

Three-day back trajectories arriving at 3000 m over GV7 at 12UTC were computed daily. The backward trajectories were generated using the Hybrid Single-Particle Lagrangian Integrated Trajectory (HYSPLIT) model developed by NOAA and Australia's Bureau of Meteorology (Draxler and Rolph, 2012), for the period spanning from 2007 to 2012, covering the snow pit time range. HYSPLIT is initialised with the European Centre for Medium Range Weather Forecast (ECMWF) ERA Interim Reanalysis meteorological data fields (Simmons et al., 2006) with a regular grid of 1° × 1°. Errors in TJ calculations after 3 days are estimated in the range 10–20% of the travel distance (Schlosser et al. (2008), Scarchilli et al. (2011)). Each trajectory is associated to the corresponding daily value of the cumulated snowfall. Snowfall data are provided by the ECMWF ERA Interim Reanalysis with 0.5° × 0.5° spatial resolution.

3. Results and discussion

3.1. Air mass backward trajectories analysis

A k-means clustering is applying to the dataset in order to operate a classification in four clusters of the trajectories (TJs) arriving at GV7 and to point out the main paths of the air masses towards the site. The main sectors of provenance are represented by means of the mean trajectories calculated from the TJs belonging to each cluster. Moreover, the whole domain is divided into a grid of 2° × 1° (long/lat) and the percentage of number of TJ points (i.e. number of hours) was calculated for each pixel (Fig. 2).

In Fig. 2 the means TJs representative of the four sectors (PLATEAU, Western Pacific Ocean-WPO, Indian Ocean - IO and Ross

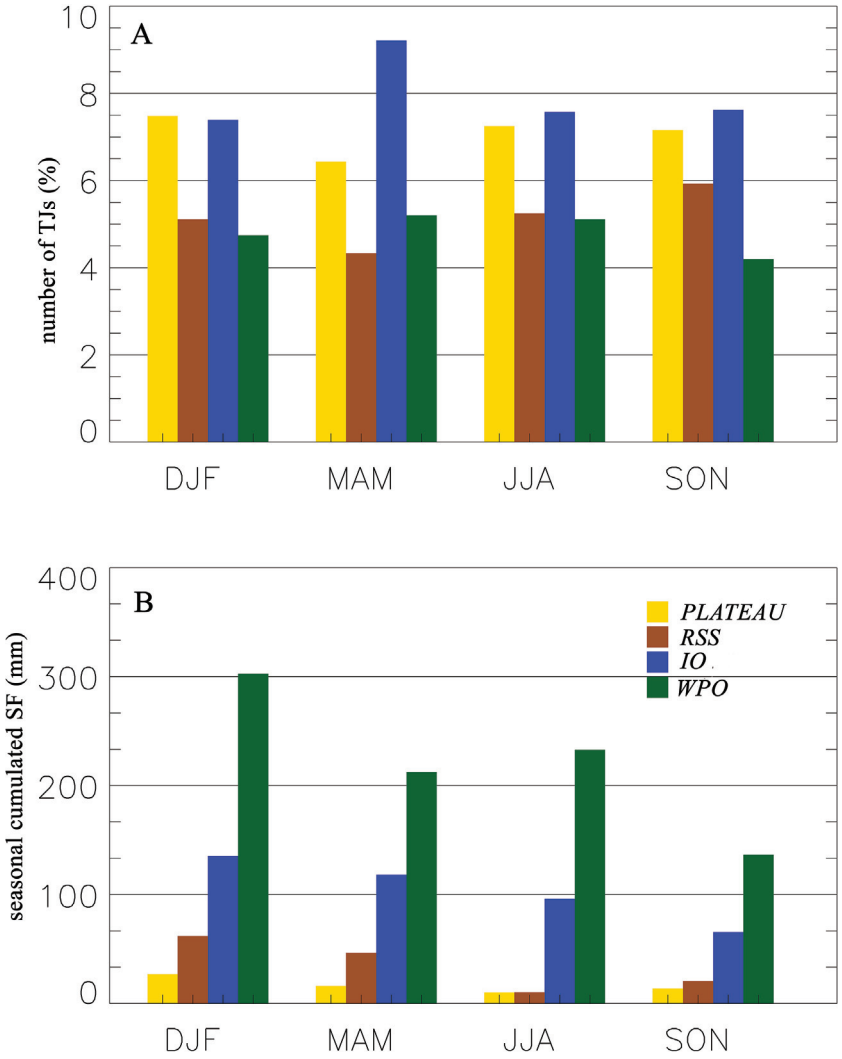

Fig. 3. Seasonal number of trajectories (%) and seasonal cumulated snowfall (mm) (A and B, respectively) related to the Plateau, Ross Sea Sector-RSS, Indian Ocean-IO and Western Pacific Ocean-WPO cluster (gold, brown, blue and green filled bars, respectively) as defined by the k-means clustering analysis. DJF, MAM, JJA and SON represent summer, autumn, winter and spring months respectively. (For interpretation of the references to colour in this figure legend, the reader is referred to the web version of this article.)

Sea Sector - RSS) are superimposed.

As illustrated in Fig. 2, during the period 2007–2013, the highest number of TJs (32%) originates from IOS followed by TJs coming from the interior (28%). Although the Western Pacific is characterized by the lowest number of TJs (19%), the air masses coming from WPO are associated to the highest value of the annual averaged cumulated snowfall (147 mm) with the respect to 69 mm brought from the Indian Ocean sector and 11 mm from the interior of the continent (see Fig. 2).

Seasonally, the number of TJs for the 4 sectors is equally distributed except for the autumn (MAM) where WPO and IO present a maximum while RSS and the PLATEU show a minimum (Fig. 3).

The cumulated snowfall seasonally averaged reaches higher values in summer and autumn (DJF and MAM) for each sector while WPO present also a second maximum in winter (JJA) (Fig. 3).

The contribution in mm w.e. of each TJ is obtained as the total cumulated snowfall, associated to each sector, divided by the related number of TJs. The contribution of the WPO is the highest due to few but intense events, bringing 2 mm w.e./TJs while the contribution of RSS and IO is lesser then 0.6 mm w.e. Obviously, TJs associated to the PLATEAU sector show an almost zero contribution (Fig. 3).

3.2. Stratigraphic profiles of chemical and isotopic parameters

3.2.1. δ^2H e $\delta^{18}O$

Oxygen and hydrogen stable isotope records in ice cores have been widely used as temperature proxies; the isotopic content in Antarctic precipitation shows a good linear correlation with surface air temperature (Stenni et al., 2016) and the snow layers can thus be considered as a continuous record of the temperature during consecutive precipitation events, assuming limited snow post-depositional processes have occurred. Moreover, the δ/T correlation may be characterized by significant spatial and temporal variability (Masson-Delmotte et al., 2008), for this reason the δ/T correlation for the GV7 area has been studied in a preliminary survey (Becagli et al., 2004).

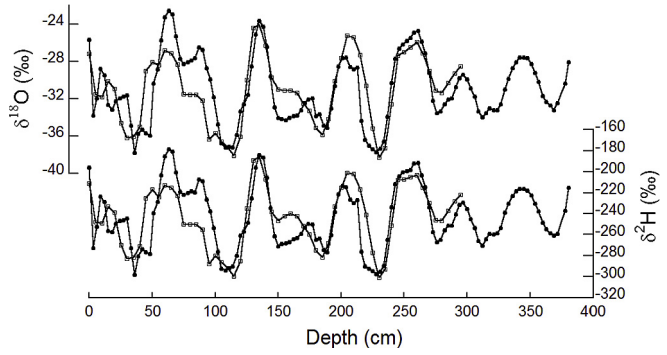

Fig. 4. $\delta^{18}O$ and δD of the GV7 snow pits. Solid dots represent the IT-SP, while the empty squares represent the ROK-SP.

The relatively high accumulation rate at GV7 is sufficient to obtain a good signal-to-noise ratio and a seasonal resolution for the upper part of the snow layers. The $\delta^{18}O$ record (δ^2H) of IT-SP is characterized by an average value of −31.14‰ (−244.32‰), while the maximum, −55.53‰ (−178.50‰) is reached at 63 cm of depth (top depth) and the minimum, −37.76‰ (−298.07‰) is observed at 36 cm (Fig. 4). The most negative values are caused by lighter winter precipitation, while the peaks belong to summer snow events, occurring at higher temperatures; the annual layers, described by the oscillations due to summer maxima and winter minima, appear to be well preserved throughout the snow pit (Fig. 4). Post-depositional effects are minimized by the relatively high accumulation rate and the temperature well below the melting point through all the year.

The IT-SP and ROK-SP were dug 10 m apart from each other, and show a good agreement of the isotopic records, characterized by almost identical seasonal oscillations. Some minor differences can be observed, mostly close to the surface, mainly due to the spatial variability that may occur within a short distance in the snow cover, which can be attributed mainly to the irregular snow accumulation on the ground and to the redistribution of light-density Antarctic surface snow operated by the wind (Frezzotti et al., 2007). The slightly different sampling resolution (3 cm for the IT-SP, 5 cm for the ROK-SP) could also results in isotopic discrepancies.

Due to this clear seasonal pattern, $\delta^{18}O$ (and/or δ^2H) will be used for stratigraphic dating, together with nssSO_4^{2-} (see section 3.3).

3.2.2. Deuterium excess

Deuterium excess is mainly influenced by the kinetic processes occurring during the evaporation of seawater and during the snow formation, and it is believed to be preserved during the moisture path (Merlivat and Jouzel, 1979). The deuterium excess is mainly driven by the climatic conditions occurring at the main moisture source regions: sea surface temperature, relative humidity and wind speed (Merlivat and Jouzel, 1979). However, the values are also influenced by the final condensation temperature occurring at the snow deposition site. The deuterium excess can give us information on moisture transport/precipitation and mass trajectories changes considering the deuterium excess an integrated tracer of hydrological cycle changes. Up to now it has been difficult to disentangle the different factors affecting the deuterium excess. Recent studies suggest the relative humidity at the moisture source as the main driver of *d* variability (Pfahl and Sodemann, 2014).

The deuterium excess record is reported in Fig. 5, for the IT-SP it has an average value of 4.79‰; the maximum (9.68‰) is located at 2.60 m of depth (top depth), while the minimum (−2.51‰) is at 3 cm. The $\delta^{18}O$ (or δ^2H) and *d* records appear phase shifted as already observed in other Antarctic coastal sites (Delmotte et al., 2000; Schlosser et al., 2008). There is a reasonably good agreement between the IT-SP and the ROK-SP *d* records.

3.2.3. Sea spray components

Sea spray is one of the main sources of atmospheric aerosol in Antarctica, especially in coastal sites (Benassai et al., 2005). Sea spray components, marked by Na^+, Cl^-, Mg^{2+} and a part of total

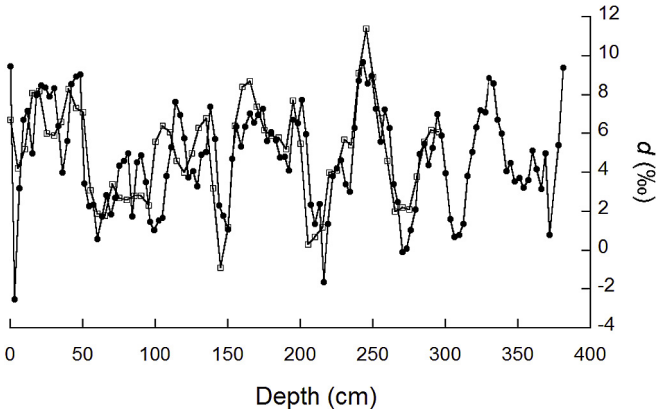

Fig. 5. Deuterium excess records from GV7 snow pits. The solid dots represent the IT-SP, the empty square the ROK-SP.

SO_4^{2-}, show wider spatial and temporal variations than the other components in the snow (Benassai et al., 2005).

Fig. 6 shows the concentration vs. depth profiles of sea spray markers, Na^+, Cl^- and Mg^{2+}. They present very similar profiles, also considering the two different snow pits.

Some in-phase concentration spikes are present; they could be related to intense sea storm events over the open ocean or to the supply of salt-enriched frost structures over sea ice transported inland by strong wind (Rankin et al., 2002; Yang et al., 2008; Abram et al., 2013). Even if a clear seasonal pattern is not visible for these markers, Fig. 6 shows that the most intense spikes occur in autumn-winter time when the percentage of trajectories from WPO sector delivering precipitation, shows high values (Fig. 3). Previous work shown that sea spray aerosol is wet deposited in coastal areas of Antarctica (Benassai et al., 2005). Therefore, in autumn-winter the sea spray aerosol is transported by air masses delivering precipitation from the oceanic sector facing GV7 and deposited at GV7 by wet precipitation. Sodium, compared to chloride and magnesium, is a more reliable marker for sea spray both due to the relatively lower importance (or absence, in very coastal stations) of extra-sea-salt sources and to the lack of fractionation phenomena occurring during transport or even after deposition (e.g. Benassai et al., 2005; Traversi et al., 2004).

By calculating ss and nss fraction for Na^+ as reported above, we noticed that $ssNa^+$ is largely dominant with respect to its non-sea-salt fraction ($nssNa^+$), accounting for 90% of total Na^+. This result is expected for this coastal site affected by precipitation coming from the fast delivering of air masses from the surrounding Ocean. In order to highlight possible additional sources for Cl^- and Mg^{2+}, in Table 1 the results of the linear correlation Cl^- vs $ssNa^+$ and Mg^{2+} vs $ssNa^+$ are reported.

Table 1 shows that all the correlations are highly significant (higher than 99% of significance), demonstrating the common source of these components from primary sea spray. Indeed, the slopes of the regression lines Cl^- vs $ssNa^+$ and Mg^{2+} vs $ssNa^+$ are near to the values 1.81 w/w and 0.12 w/w, representing the theoretical Cl^-/Na^+ and Mg^{2+}/Na^+ ratios in sea water.

The intercept of Cl^- vs $ssNa^+$ regression lines is well above 0 (about 5 and 10 μg L^{-1} for IT-SP and ROK-SP, respectively) pointing to the presence of an extra source of HCl from background long range transport. This extra source could be related to direct volcanic emissions or to the formation of gaseous HCl as a consequence of acid–base chemical exchange between NaCl and HNO_3 or H_2SO_4 in the atmosphere (Legrand and Delmas, 1988).

The slope of the Mg^{2+} vs $ssNa^+$ regression line is slightly below the theoretical sea water ratio and the intercept is negligible, demonstrating that, in spite of being one of the most abundant components of upper continental crustal, at this site Mg^{2+} is predominantly associated to primary sea spray.

3.2.4. Dust

The concentration of total and insoluble dust against the depth is reported in Fig. 7 together with $\delta^{18}O$ profiles. Insoluble particles are measured along the whole depth interval covered by the KOR-SP (Fig. 7). Superimpose to a seasonal patter with spring maxima, a decreasing trend in the insoluble particle concentration from the surface to the bottom of the snow pit is observed. For the depth range analysed by both the two groups a very good agreement

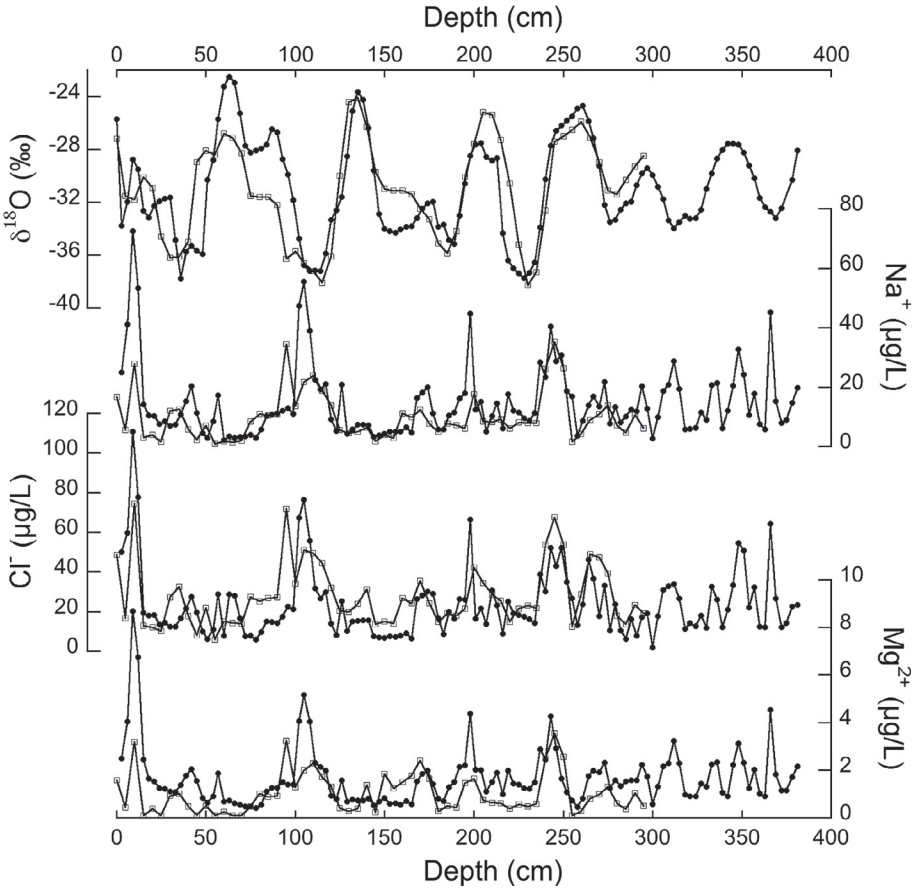

Fig. 6. Concentration vs. depth profiles of sea spray markers (Na^+, Cl^- and Mg^{2+}) in comparison with $\delta^{18}O$. Italian snow pit (IT-SP) is shown with solid dots, Korean snow pit (ROK-SP) with empty squares.

Table 1
Slope, intercept, R, number of samples (n) and significance level (p) of the linear regressions between Cl^- vs $ssNa^+$ and Mg^{2+} vs $ssNa^+$ for the Italian and Korean snow pits (IT-SP and ROK-SP, respectively). * Bowen, 1979.

	IT-SP		ROK-SP	
	Cl^- vs. $ssNa^+$	Mg^{2+} vs. $ssNa^+$	Cl^- vs. $ssNa^+$	Mg^{2+} vs. $ssNa^+$
Sea water ratio	1.81*	0.12*	1.81*	0.12*
Slope	1.36 ± 0.04	0.10 ± 0.00	1.83 ± 0.10	0.10 ± 0.01
Intercept	5.08 ± 0.77	0.35 ± 0.05	9.96 ± 1.23	0.06 ± 0.08
R	0.9444	0.9581	0.9269	0.8925
n	127	127	60	60
p	<0.01	<0.01	<0.01	<0.01

between the insoluble particles concentration measurements is visible. Besides, the depth profiles of total and insoluble particles show a common pattern. When considering particles between 600 nm and 10 μm (equivalent spherical diameter), the insoluble fraction represents, on average, 50–60% of total particles.

Both total and insoluble dust concentration profiles appear to anticipate the $\delta^{18}O$ signal, therefore eolian particles probably reach GV7 site during the end of winter (minimum $\delta^{18}O$ values) and their maximum concentration occurs during spring (when $\delta^{18}O$ values increase), and then gradually decrease in summer.

This difference is attributed to the varying particles deposition and not to seasonal snow accumulation variability, this latter changing only by ~10% (Frezzotti et al., 2007).

GV7 snow pit insoluble particle record, with its seasonal variability, is likely related to atmospheric circulation patterns affecting coastal East Antarctica. The increase of insoluble aerosols concentrations during the spring season and the maxima during summer may be related to the high mesoscale cyclonic activity in the Ross Sea; air masses travelling from the Ross Sea to GV7 above Northern Victoria Land mobilize mineral dust from ice-free areas of the Transantarctic mountains that are transported and then deposited at GV7. Similar results were presented in Delmonte et al. (2013) for Talos Dome site. Backward trajectories analysis shows a higher number of trajectories from the Ross Sea sector in spring (RSS in SON in Fig. 3). As dust is dry-deposited the trajectories delivering dust are not related to snowfall events. On the other hand, backward trajectories analysis show that during winter air masses reaching GV7 mainly derive from the Plateau and IO sectors, thus bringing air masses enriched at least in humidity and sea spray aerosol but not in dust.

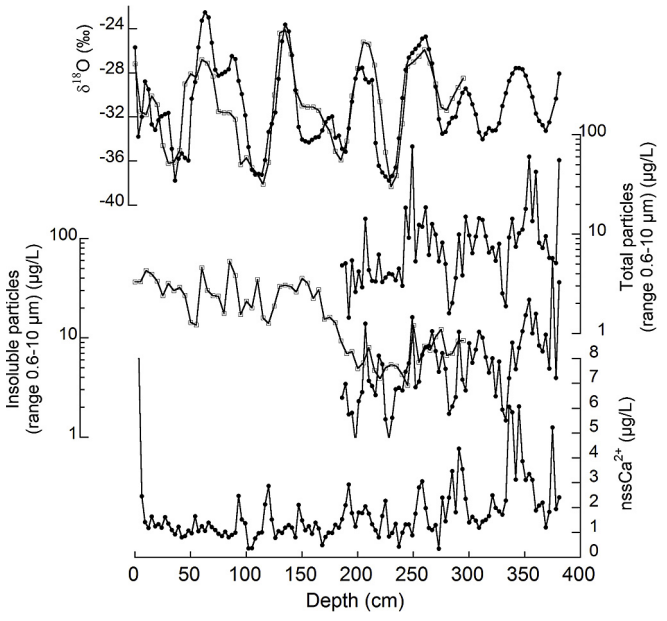

Fig. 7. Concentration vs. depth profiles of particles in dust, with total particles (0.6–10 μm), insoluble particles (0.6–10 μm), and $nssCa^{2+}$, in comparison with $\delta^{18}O$. Italian snow pit (IT-SP) is shown with solid dots, Korean snow pit (ROK-SP) with empty squares.

Among the soluble ions, Ca^{2+} is usually taken as the most reliable marker of mineral dust, although it arises also from sea spray. For this reason, it is important to define the non-sea-salt Ca^{2+} ($nssCa^{2+}$) fraction calculated as shown above in the two-equation system (section 2.4). At this site, non-sea-salt calcium is dominant with respect to Ca^{2+} arising from sea spray, $nssCa^{2+}$ represents about 75% of total calcium.

$NssCa^{2+}$ presents concentrations about one order of magnitude lower than insoluble particles and its concentrations are not significantly correlated with those of total and insoluble particles. $NssCa^{2+}$ determined by ion chromatography represents about 42% of soluble dust, the latter calculated as the difference between total and insoluble particles. Calcium in Antarctic dust is usually present in the form of $CaSO_4$, $Ca(NO_3)_2$ and $CaCO_3$ (Iizuca et al., 2013). The percentage of $nssCa^{2+}$ in soluble dust suggests that its main Ca bearing component is $CaCO_3$. Indeed, in $CaCO_3$ Ca represents 40% in terms of mass. It has to be noticed that the Ca^{2+} concentration is very low in GV7 snow samples, well below the solubility constant of $CaCO_3$. Besides, the acidic character of the snow layers (see below section 3.4) increses the solubility of $CaCO_3$. In this way the presence of $CaCO_3$ in the soluble part of dust is possible. The presence of calcium carbonate in snow layers at Talos Dome - not far from GV7- has been already documented by Sala et al. (2008), supporting our findings.

3.2.5. *Biogenic sulfur oxidized compounds (MSA and $nssSO_4^{2-}$)*

In this section, depth profiles of sulfur oxidized compounds (non-sea-salt sulfate, $nssSO_4^{2-}$ and methanesulfonic acid, MSA) are shown; they arise from the atmospheric oxidation of dimethyl sulfide (DMS), the most abundant sulfide organic compound in nature, derived from metabolic processes of marine phytoplanktonic species (e.g. Becagli et al., 2016).

MSA is only produced by biological marine life, while $nssSO_4^{2-}$ arises from other sources such as volcanic and anthropogenic emissions or crustal erosion. As there aren't evidences of volcanic eruptions recorded in the snow layers in the time period covered by the snow pit and the crustal and anthropic sources of sulfate are negligible in Antarctica (e.g. Becagli et al., 2005), it can be assumed that $nssSO_4^{2-}$ arise only by biogenic source.

The strong seasonality of DMS production leads to an analogous seasonal behavior of MSA and $nssSO_4^{2-}$, with maximum concentrations during phytoplanktonic bloom. Fig. 8 shows that MSA and $nssSO_4^{2-}$ summer peaks are coincident with maxima in $\delta^{18}O$, even if sometimes MSA came slightly after the $\delta^{18}O$ and $nssSO_4^{2-}$ maxima. MSA and $\delta^{18}O$ can potentially be affected by diffusion in the firn, due to snow-vapor interactions (Johnsen, 1977; Mulvaney et al.,

1998).

Besides, high temporal resolution studies in the Antarctic plateau show that for MSA and nssSO_4^{2-} the temporal dynamic in summer is not the same. This different behavior is attributed both to the different rate of photochemical oxidation of the two species (Preunkert et al., 2008) and to the different size distribution and transport pathways during early spring and summer (Becagli et al., 2012).

The seasonal cycle for all the three parameters is regular along the entire snow pit and these parameters are useful for snow pit dating. The in phase seasonal pattern between the two components is maintained for deep snow layers as shown in Fig. 9 for the 12 m GV7-D firn core. Fig. 9b shows that some summer maxima in the MSA profiles are less evident than nssSO_4^{2-} profiles (Fig. 9a), for this reason nssSO_4^{2-} are chosen for annual counting. Fig. 9b also shows that even considering a longer record than snow-pit there is not a decreasing trend in MSA concentration as depth increases. This evidence demonstrates that MSA is a reliable marker for reconstruction of past environmental changes at this site.

The agreement between these seasonal proxies measured on the two snow pits (Fig. 8) supports the goodness of the records from the two laboratories and the undisturbed accumulation at GV7 site.

All these results are of particular relevance as they allow to date and reconstruct the environmental variability for longer time period by the analysis of the 250 m ice core drilled in the same site.

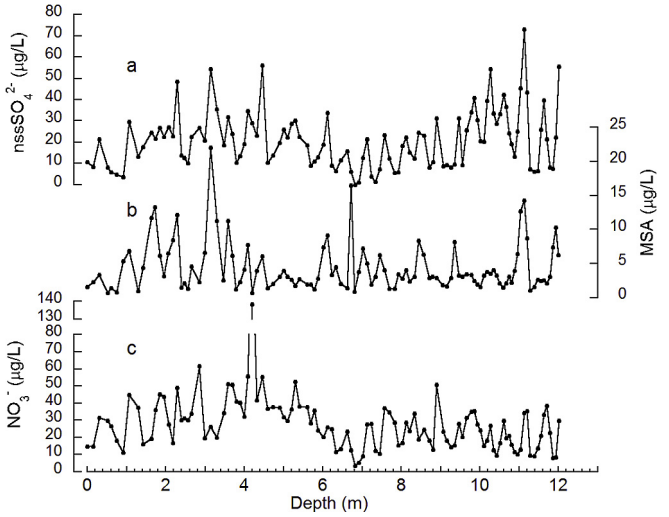

Fig. 9. Concentration vs. depth profiles of nssSO_4^{2-} (plot a), MSA (plot b) and NO_3^- (plot c) for the12 m firn core GV7-D drilled in parallel to the snow pits.

3.2.6. NO_3^-

Nitrate is one of the main components of Antarctic deposited aerosol. It arises mainly from stratosphere/troposphere interchanges, lightning and other photo-induced atmospheric processes. Its atmospheric distribution is related to its presence in the aerosol gaseous phase as acidic species (HNO_3). Such behavior is consistent with the seasonal character of nitrate sources and transport mechanisms, which are enhanced in spring/summer periods when a more efficient stratosphere/troposphere exchange and higher irradiance flux (needed for an efficient oxidation of nitrogen oxides) occur (Legrand and Delmas, 1986; Traversi et al., 2004; Traversi et al., 2014)).

Nitrate appears to be well preserved in snow layer (Fig. 10) as expected for this high accumulation site (Traversi et al., 2012) but a clear seasonal patter with maxima in phase with nssSO_4^{2-} and $\delta^{18}O$ is not visible along all the snow pit. For this reason NO_3^- is not used for annual layer counting.

Fig. 9 shows the NO_3^- concentration along the 12 m firn core. As already observed for MSA also NO_3^- does not show any concentration decreasing trend as depth increses. Therefore, NO_3^- record at GV7 site can be used for past environmental change reconstruction.

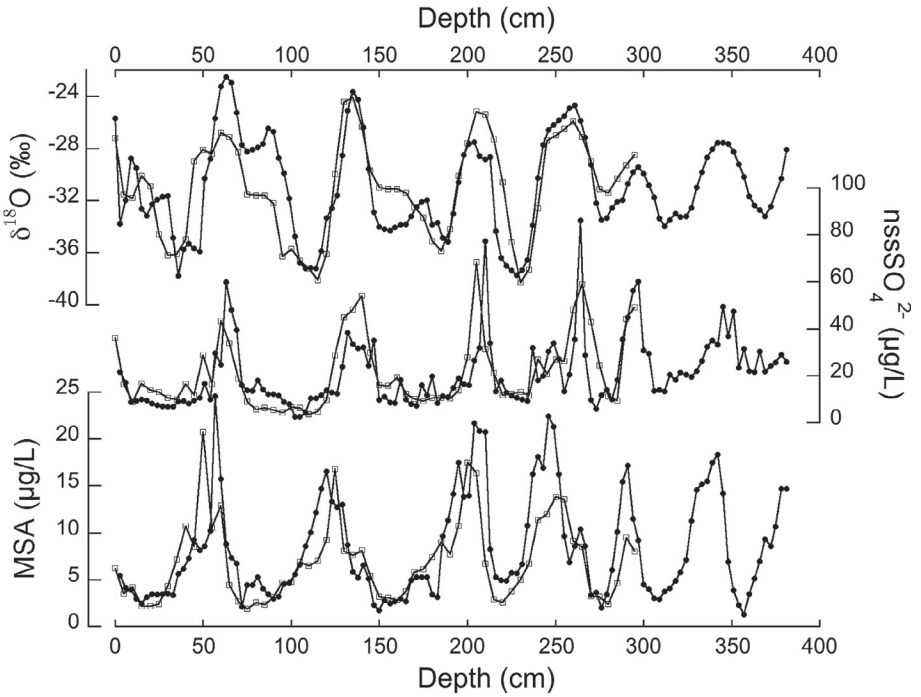

Fig. 8. Concentration vs. depth profiles of sulfur oxidized compounds (nssSO_4^{2-} and MSA) in comparison with $\delta^{18}O$. Italian snow pit (IT-SP) is shown with solid dots, Korean snow pit (ROK-SP) with empty squares.

3.2.7. Bromine and iodine

These parameters are determined only in the Italian laboratory on the samples from the IT-SP.

Bromine and iodine arise from sea spray, but in snow layers bromine and iodine result enriched with respect to sea water composition. The bromine and iodine enrichment are related to photochemical recycling of bromine (bromine explosion) happening in the Austral spring season over sea ice with the recovery of solar radiation (Spolaor et al., 2014, 2016, Yang et al., 2008).

At coastal locations, bromine and iodine are more enriched with respect to sea salt compositions than at inner sites, as they are progressively depleted as air masses travel further inland.

The determination of the seasonal pattern and evolution of bromine and iodine at the costal high accumulation site of GV7 is of particular relevance in order to understand the seasonal timing of Br_{enr} and I_{enr} and their possible link with sea ice extent in spring.

Fig. 11 reveals a common pattern for Br_{enr} and I_{enr} in GV7 snow pit, while a clear seasonal pattern is not evident. The maximum at around 140 cm depth recorded in both Br_{enr} and I_{enr} likely occurs during the austral late spring as it slightly anticipates the maximum in $\delta^{18}O$. This timing was already observed in other Antarctic ice core archives (such as Talos Dome; Spolaor et al., 2014; Law Dome; Vallelonga et al., 2016), but need to be confirmed by longer time series for GV7 site. Further studies are also necessary to understand why the maxima in Br_{enr} and I_{enr} are not evident every year.

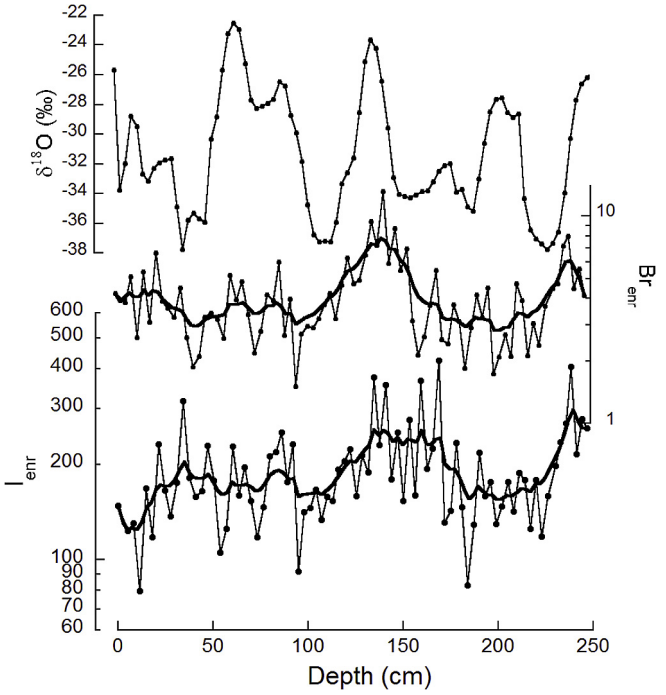

Fig. 11. Concentration (log scale) vs. depth profiles of bromine enriched and iodine enriched in comparison with $\delta^{18}O$. The overlapped bold lines in Br_{enr} and I_{enr} plots represent the smoothed profiles.

3.2.8. Refractory black carbon (rBC)

Black carbon (BC) is a kind of carbonaceous aerosol, which is emitted during the combustion of fossil fuels and biomass, characterized by a small diameter (from tens to hundreds nanometers) and a notable atmospheric stability (Bond et al., 2013).The most relevant sources of BC for the Antarctic atmosphere during the austral winter/spring are the Australian and South American biomass and fossil fuels burning emissions (Stohl and Sodemann, 2010; Li et al., 2008). Moreover, the West Antarctica aerosol loadings are strongly influenced by the Australian emissions of BC and dust (De Deckker et al., 2010).

Seasonal oscillations in the atmospheric BC concentrations were measured in the Antarctic continent, generally showing a maximum in October, as measured at Halley (Wolff and Cachier, 1998), Ferraz (Pereira et al., 2006), Neumayer (Weller et al., 2013) and Amundsen-Scott (Bodhaine, 1995) stations.

Ice cores record (covering the period 1850–2000 AD) revealed the primary role of the intensity of emissions at the sources and the meridional atmospheric transport in explaining the rBC variability (Bisiaux et al., 2012). Particularly, El Niño Southern Oscillation indirectly contributes in explaining the 5–6 years modulation in the rBC deposition, by controlling the continental hydrology and the fire regime (Bisiaux et al., 2012).

The rBC mean concentration measured in the GV7 snow pit samples is of 0.097 $\mu g\ L^{-1}$ with a standard deviation of 0.091 $\mu g\ L^{-1}$, which is in good agreement with previous ice core studies results (Bisiaux et al., 2012). The rBC snow-pit record (Fig. 12) does not

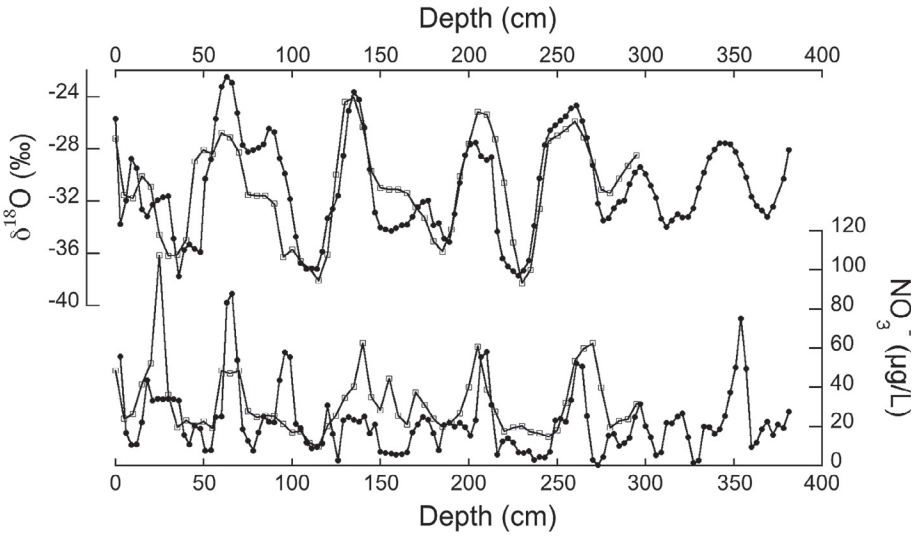

Fig. 10. Concentration vs. depth profile of nitrate in comparison with $\delta^{18}O$. Italian snow pit (IT-SP) is shown with solid dots, Korean snow pit (ROK-SP) with empty squares.

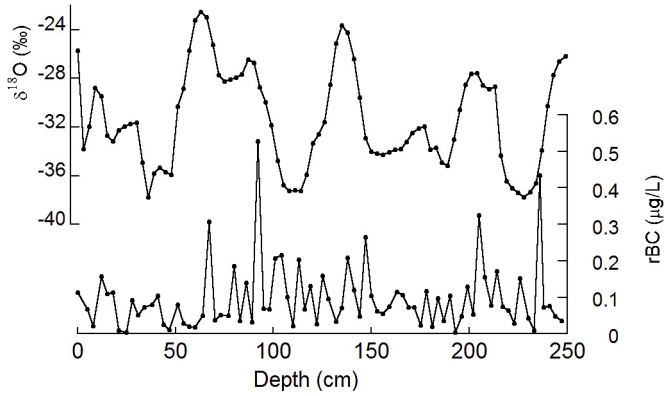

Fig. 12. IT-SP concentration vs. depth profiles of rBC in comparison with $\delta^{18}O$.

show a clear seasonal pattern, but rBC concentration spikes occur mainly in summer.

It is possible to speculate that the highest rBC concentrations observed in the 75–100 cm depth range and corresponding to the summer 2012 (see Fig. 13 in the section 3.3) might be the result of the Australian wild fire regime, significantly stronger than average due to the abundant grass growth of the two previous years, characterized by La Niña events (BushfireCRC, 2013; Bushfire_Bulletin, 2013). Particularly, the highest rBC peak (about 0.5 μg L^{-1}) was measured in the austral summer period, in correspondence to a heat wave with temperatures among the highest ever recorded in Australia (Australian Government Bureau of Meteorology).

3.3. Dating and accumulation rate

The dating of a snow pit or ice/firn core is the basis for a correct interpretation of climate information and for the comparison with other climate records. This is why temporal trends of snow pits and ice/firn cores have always been a topic of great interest and it is what pushes to research for more and more precise, accurate and highly resolved records.

Thanks to the high accumulation rate characterizing GV7, an accurate dating of the snow pit is allowed, by counting successive annual snow layers, whose succession is suggested by those markers presenting a clear seasonal trend along the stratigraphy, or by the presence of specific dated events (e.g. volcanic eruptions).

At GV7 several markers with clear seasonal characters are found: δ^2H, $\delta^{18}O$, $nssSO_4^{2-}$, MSA. As above discussed, $nssSO_4^{2-}$ and $\delta^{18}O$ are chosen for dating purpose because both their maxima occur during the same months (January–February, i.e. full-late summer), $nssSO_4^{2-}$ and ^{18}O concentration vs depth profiles are shown in Fig. 13.

The annual counting starts at the surface from December 2013 (the time of sampling). For the IT-SP 4 m snow pit it is possible to identify 7 summer peaks with high accuracy (Fig. 13). The first 6 peaks coincide with the maxima recorded in the 3 m long KOR-SP (Fig. 13).

Thanks to this dating, it is possible to perform a calculation of both annual and average accumulation rates (Fig. 14). On average, the mean accumulation rate ranges from 242 ± 71 mm w.e. for the IT-SP and 250 ± 85 mm w.e. for the ROK-SP. These values are in good agreement each other even if referring to slightly different time period (2007–2013 and 2008–2013); moreover the pattern of the year accumulation rate is similar in the two snow pits (Fig. 14).

The average accumulation rates found in this work are in excellent agreement with the value of 241 ± 13 mm we yr^{-1} measured in previous work by Magand et al. (2004) and Proposito and Frezzotti (2008) for the period 1965–2001.

3.4. Ionic balance

The seasonal trend of the markers shown in the previous sections can be summarized by the overall composition in the two main seasons. At this purpose the ion balance calculated in "summer" and "winter" furnishes an overview of the average ionic load and acidity in the snow layers at GV7 in the two seasons.

Following the seasonal trends achieved by $nssSO_4^{2-}$ samples are split in summer and winter samples by considering the mean values of $nssSO_4^{2-}$ as threshold.

The acidic or alkaline character of the snow layers is assessed by the unbalance between anionic and cationic content. The anionic excess is ascribed to the presence of H^+, while the cationic excess is explained by the presence of HCO_3^-/CO_3^{2-}, because they are usually not determined directly by Ion Chromatography (Legrand and Delmas, 1984).

Ion balances reported in Fig. 15 show that the total ionic load is larger during summer than during winter period. The higher ionic load in summer is mainly due to the secondary aerosol species: sulfate, nitrate and MSA. As above described also dust (expressed in the ionic balance by Ca^{2+}) and halogens (not visible in the picture due to their low concentrations) present higher concentration in summer than in winter. These anionic species are only partially

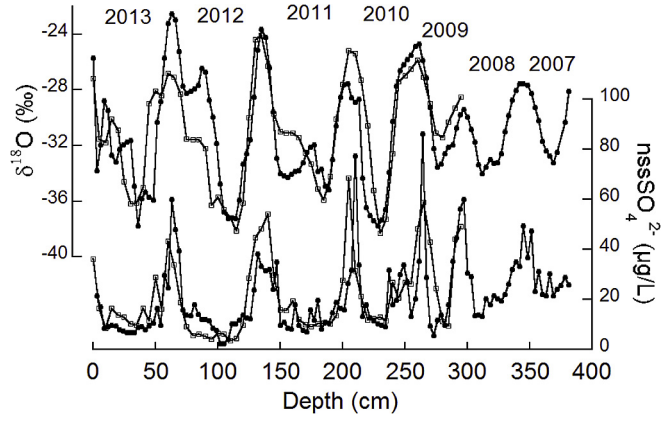

Fig. 13. Dating of the snow pits, with the comparison between $\delta^{18}O$ and $nssSO_4^{2-}$. Italian snow pit (IT-SP) is shown with solid dots, Korean snow pit (ROK-SP) with empty squares.

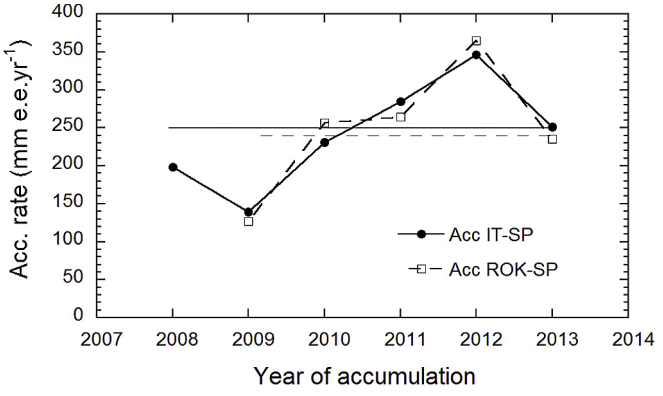

Fig. 14. Temporal trend of yearly accumulation rate for IT-SP and ROK-SP. The continue and dashed horizontal lines represent the mean accumulation rates for IT-SP and ROK-SP respectively.

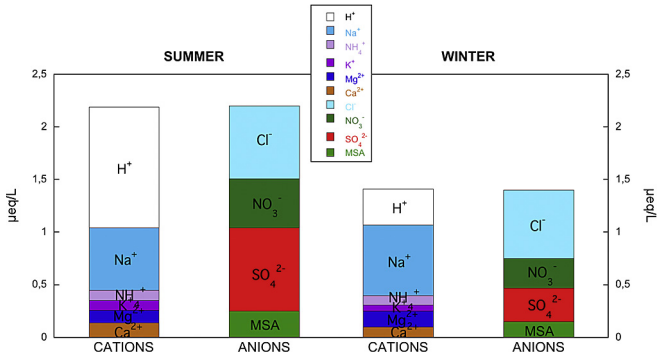

Fig. 15. Average ion balances of the snow pits during summer and winter periods. Concentrations are expressed as μeq L^{-1}.

neutralised by cations, conferring to the snow an acidic character, much higher during summer than in winter.

The ionic composition in winter is characterized by concentration and contribution of sea spray species higher than in summer. Besides, due to a lower concentration of sulfate, MSA and nitrate a lower acidity is measured in this season.

4. Summary and conclusions

In this work we have shown an extensive chemical data set obtained by the analysis of snow-pit samples from a coastal site (GV7) in the East Antarctic ice sheet. The chemical data set is compared with stable isotope composition and seasonal cluster backward trajectories analysis in order to highlight and interpret as function of air masses provenance the seasonal pattern of each marker and their potentiality to reconstruct past environmental and climatic changes by the chemical analysis of a 250 m ice core drilled at the same site.

The main results of this study may be summarized as follows:

- The number of back trajectories for the clustered 4 sectors (Plateau, Western Pacific Ocean, Indian Ocean and Ross Sea) are equally distributed except for the autumn where Indian Ocean present a maximum. The cumulated snowfall seasonally averaged reaches higher values in summer and autumn for each sector while Western Pacific Ocean presents a second maximum in winter;
- δ^2H e $\delta^{18}O$ appear to be well preserved throughout the snow-pit showing a clear seasonal pattern. Post-depositional effects are minimized by the relatively high accumulation rate and the temperature well below the melting point through all the year;
- $ssNa^+$ account for about 90% of total Na^+, it is significantly correlated with Cl^- and Mg^{2+} with slope similar to sea water composition. Sea spray aerosol is delivered together with snow precipitation especially in winter by air masses arising from west Pacific Ocean sector. Chloride depletion is not observed likely due to the vicinity of the oceanic source and the fast advection of air masses delivering sea salt aerosol.
- the total and insoluble dust show sometimes maximum concentration in early spring when the circulation pattern of air masses from Ross Sea sector mobilize mineral dust from ice-free areas of the Transantarctic mountains toward GV7 site. $CaCO_3$ is the main compound of soluble dust;
- as expected the Sulfur oxidized compounds (MSA and $nssSO_4^{2-}$) have a clear seasonal pattern with maximum concentrations in summer when a large phytoplanktonic bloom occur in the surrounding ocean. The seasonal pattern is preserved in deep snow layers as revealed by the analysis of a 12 m firn core;
- MSA and NO_3^- do not show any concentration decreasing trend as depth increases, also considering a longer record obtained by the 12 m firn core. This evidence demonstrates that these two compounds are preserved in the snow layers and can be considered reliable markers for the reconstruction of past environmental changes at this site.
- Br_{enr} and I_{enr} do not show a regular seasonal pattern, but along the snow pit the main maximum in the record occur in spring when the photochemical recycling of bromine (bromine explosion) occurs over sea ice. The role of these markers in reconstruct past sea ice extent variation in spring season need to be further investigated.
- Refractory black carbon (rBC) is a very important marker for biomass burning source but it is not usually determined in the snow layers due to its very low concentration in this matrix. The record of rBC show several concentration spikes especially in summer. In particular, the highest concentration (0.5 μg L^{-1}) is recorded in summer 2012. It is likely related to large biomass burning evens occurs in Australia in correspondence to the 2012 heat wave. This marker reveals to be a potential indicator of the past occurrence of biomass burning events in Australia by the analysis of the deep ice core drilled in this site.
- the ionic balance reveals high ionic load and acidity in summer samples due to the higher concentration of H_2SO_4 and MSA from biogenic source and HNO_3 arising from stratosphere/troposphere interchanges, lightning and other photo-induced atmospheric processes.
- the comparison between the stratigraphies and the accumulation rate trend of two snow pits dug 10 m distance apart from and analysed in Italian and Korean laboratory, reveals a very good agreement between the time series, demonstrating the presence of an undisturbed accumulation rate at this site.
- The average annual accumulation rate for the period 2008–2013 is 242 ± 71 mm w.e..

Finally all these evidence highlight the importance of this site to give information at high temporal resolution on the climatic variability in the last millennium by the chemical and isotopic analysis on the 250 m ice core drilled in this site.

Acknowledgment

This research was financially supported by the MIUR (Italian Ministry of University and Research) - PNRA (Italian Antarctic Research Programme) program through the IPICS-2kyr-It project (International Partnership for Ice Core Science, reconstructing the climate variability for the last 2kyr, the Italian contribution).The IPICS-2kyr-It project is carried out in cooperation with KOPRI (Korea Polar Research Institute, grant No. PE15010).

References

Abram, N., Wolff, E.W., Curran, M.A.J., 2013. A review of sea ice proxy information from polar ice cores. Quat. Sci. Rev. 79, 168–183.

Agosta, C., Favier, V., Krinner, G., Gallée, H., Fettweis, X., Genthon, C., 2013. High-resolution modelling of the Antarctic surface mass balance, application for the twentieth, twenty first and twenty second centuries. Clim. Dyn. 41, 3247–3260.

Australian Government Bureau of Meteorology: http://www.bom.gov.au/cgi-bin/climate/change/extremes/timeseries.cgi?graph=HD35&ave_yr=0.

Becagli, S., Lazzara, L., Marchese, C., Dayan, U., Ascanius, S.E., Cacciani, M., Caiazzo, L., Di Biagio, C., Di Iorio, T., di Sarra, A., Eriksen, P., Fani, F., Giardi, F., Meloni, D., Muscari, G., Pace, G., Severi, M., Traversi, R., Udisti, R., 2016. Relationships linking primary production, sea ice melting, and biogenic aerosol in the Arctic. Atmos. Environ. 136, 1–15. http://dx.doi.org/10.1016/j.atmosenv.2016.04.002.

Becagli, S., Proposito, M., Benassai, S., Flora, O., Genoni, L., Gragnani, R., Largiuni, O., Pili, S.L., Severi, M., Stenni, B., Traversi, R., Udisti, R., Frezzotti, M., 2004. Chemical and isotopic snow variability in East Antarctica along the 2001/02 ITASE traverse. Ann. Glaciol. 39, 473–482.

Becagli, S., Proposito, M., Benassai, S., Gragnani, R., Magand, O., Traversi, R., Udisti, R., 2005. Spatial distribution of biogenic sulphur compounds(MSA, nssSO42-) in the northern Victoria Land - Dome C- Wilkes Land area (East Antarctica). Ann. Glaciol. 41, 23–31.

Becagli, S., Scarchilli, C., Traversia, R., Dayan, U., Severi, M., Frosini, D., Vitale, V., Mazzola, M., Lupi, A., Nava, S., Udisti, R., 2012. Study of present-day sources and transport processes affecting oxidised sulphur compounds in atmospheric aerosols at Dome C (Antarctica) from year-round sampling campaigns. Atmos. Environ. 52, 98–108. http://dx.doi.org/10.1016/j.atmosenv.2011.07.053.

Benassai, S., Becagli, S., Gragnani, R., Magand, O., Proposito, M., Fattori, I., Traversi, R., Udisti, R., et al., 2005. Sea-spray deposition in Antarctic coastal and plateau areas from ITASE traverses. Ann. Glaciol. 41, 32–40.

Bisiaux, M.M., Edwards, R., McConnell, J.R., Curran, M.A.J., Van Ommen, T.D., Smith, A.M., Neumann, T.A., Pasteris, D.R., Penner, J.E., Taylor, K., 2012. Changes in black carbon deposition to Antarctica from two high-resolution ice core records, 1850–2000 AD. Atmos. Chem. Phys. 12, 4107–4115. http://dx.doi.org/10.5194/acp-12-4107-2012.

Bodhaine, B.A., 1995. Aerosol absorption measurements at Barrow, Mauna Loa and the south pole. J. Geophys. Res. Atmos. 100 (D5), 8967–8975. http://dx.doi.org/10.1029/95JD00513.

Bond, T.C., Doherty, S.J., Fahey, D.W., Forster, P.M., Berntsen, T., DeAngelo, B.J., Flanner, M.G., Ghan, S., Kärcher, B., Koch, D., et al., 2013. Bounding the role of black carbon in the climate system: a scientific assessment. J. Geophys. Res. Atmos. 118, 5380–5552.

Bowen, H.J.M., 1979. Environmental Chemistry of the Elements. Elsevier, New York.

BushfireBulletin, 2013: http://issuu.com/nswrfs/docs/nsw_rfs_bush_fire_bulletin_single_page.

BushfireCRC, 2013:http://www.bushfirecrc.com/sites/default/files/managed/resource/southern_outlook_f95_final.pdf.

Caiazzo, L., Becagli, S., Frosini, D., Giardi, F., Severi, M., Traversi, R., Udisti, R., 2016. Spatial and temporal variability of snow chemical composition and accumulation rate at Talos Dome site (East Antarctica). Sci. Total Environ. 550, 418–430.

Church, J.A., Clark, P.U., Cazenave, A., Gregory, J.M., Jevrejeva, S., Levermann, A., Merrifield, M.A., Milne, G.A., Nerem, R.S., Nunn, P.D., 2013. Sea Level Change. PM Cambridge University Press.

Craig, H., 1961. Isotopic variations in meteoric waters. Science 133, 1702–1703. http://dx.doi.org/10.1126/science.133.3465.1702.

Dansgaard, W., 1964. Stable isotopes in precipitation. Tellus 16, 436–4468.

De Deckker, P., Norman, M., Goodwin, I.D., Wain, A., Gingele, F.X., 2010. Lead isotopic evidence for an Australian source of aeolian dust to Antarctica at times over the last 170,000 years. Palaeogeogr. Palaeocl. 285, 205–223.

Delmonte, B., Petit, J.R., Maggi, V., 2002. Glacial to Holocene implications of the new 27000-year dust record from the EPICA Dome C (East Antarctica) ice core. Clim. Dyn. 18 (8), 647–660.

Delmonte, B., Baroni, C., Andersson, P.S., Narcisi, B., Salvatore, M.C., Petit, J.R., Scarchilli, C., Frezzotti, M., Albani, S., Maggi, V., 2013. Modern and Holocene aeolian dust variability from Talos Dome (Northern Victoria Land) to the interior of the Antarctic ice sheet. Quat. Sci. Rev. 64, 76–89. http://dx.doi.org/10.1016/j.quascirev.2012.11.033.

Delmotte, M., Masson, V., Jouzel, J., Morgan, V., 2000. A seasonal deuterium excess signal at Law Dome, coastal eastern Antarctica: a Southern Ocean signature. J. Geophys. Res. 105, 7187–7197. http://dx.doi.org/10.1029/2007jd009190, 2008.

Draxler, R.R., Rolph, G.D., 2012. HYSPLIT (HYbrid Single-particle Lagrangian Integrated Trajectory). NOAA Air Resources Laboratory, Silver Spring. MD. Model access via NOAA ARL READY. http://ready.arl.noaa.gov/HYSPLIT.php.

EPICA Community Members, 2006. One-to-one coupling of glacial climate variability in Greenland and Antarctica. Nature 444, 195–198. http://dx.doi.org/10.1038/nature05301.

Fischer, H., Fundel, F., Ruth, U., Twarloh, B., Wegner, A., Udisti, R., Becagli, S., Castellano, E., Morganti, A., Severi, M., Wolff, E., Littot, G., Röthlisberger, R., Mulvaney, R., Hutterli, M.A., Kaufmann, P., Federer, U., Lambert, F., Bigler, M., Hansson, M., Jonsell, U., de Angelis, M., Boutron, C., Siggaard-Andersen, M.-L., Steffensen, J.P., Barbante, C., Gaspari, V., Gabrielli, P., Wagenbach, D., 2007. Reconstruction of millennial changes in dust emission, transport and regional sea ice coverage using the deep EPICA ice core from the Atlantic and Indian Ocean sector of Antarctica. Earth Planet. Sci. Lett. 260 (1–2), 340–354.

Frezzotti, M., Urbini, S., Proposito, M., Scarchilli, C., Gandolfi, S., 2007. Spatial and temporal variability of surface mass balance near Talos Dome, East Antarctica. J. Geophys. Res. 112, F02032.

Genoni, L., Stenni, B., Proposito, M., Flora, O., Braida, M., Frezzotti, M., 2008. A record of $\delta^{18}O$ variations from a near coastal site between Oates Coast and Talos Dome (East Antarctica). Terra Antarct. Rep. 14, 159–162.

Henderson, P., Henderson, G.M., 2009. The Cambridge Handbook of Earth Science Data. University Press, Cambridge, pp. 42–44. Cambridge.

Hong, S.-B., Lee, K., Hur, S.-D., Hong, S., Soyol-Erdene, T.-O., Kim, S.-M., Chung, J.-W., Jun, S.-J., Kang, C.-H., 2015. Development of melting system for measurement of trace elements and ions in ice core. Bull. Korean Chem. Soc. 36, 1069–1081.

Iizuca, Y., Delmonte, B., Oyabu, I., Karlin, T., Maggi, V., Albani, S., Fukui, M., Hondoh, T., Hansson, M., 2013. Sulphate and chloride aerosols during Holocene and last glacial periods preserved in the Talos Dome Ice Core, a peripheral region of Antarctica. Tellus B 65. http://dx.doi.org/10.3402/tellusb.v65i0.20197.

IPCC-AR5, 2013. Intergovernmental Panel for Climate Change - Fifth Assessment Report, "Climate Change 2013. The Physical Science Basis" (Summary for Policymakers).

Johnsen, S., 1977. Stable isotope homogenization of polar firn and ice. Isotopes Impurities Snow Ice 1.

Kang, J.-H., Hwang, H., Hong, S.B., Hur, S.D., Choi, S.-D., Lee, J., Hong, S., 2015. Mineral dust and major ion concentrations in snowpit samples from the NEEM site. Greenl. Atmos. Environ. 120, 137–143.

Kaspari, S., Painter, T.H., Gysel, M., Skiles, S.M., Schwikowski, M., 2014. Seasonal elevational variations of black carbon, dust in snow, ice in the Solu-Khumbu, Nepal, estimated radiative forcings. Atmos. Chem. Phys. 14, 8089–8103.

Krinner, G., Magand, O., Simmonds, I., Genthon, C., Dufresne, J.-L., 2007. Simulated Antarctic precipitation and surface mass balance at the end of the twentieth and twenty-first centuries. Clim. Dyn. 28, 215–230.

Legrand, M., Delmas, R.J., 1986. Relative contributions of tropospheric and stratospheric sources to nitrate in Antarctic snow. Tellus 38B (3–4), 236–249.

Legrand, M.R., Delmas, R.J., 1984. The ionic balance of Antarctic snow: a 10-year detailed record. Atmos. Environ. 18 (9), 1867–1874.

Legrand, M.R., Delmas, R.J., 1998. Formation of HCl in the Antarctic atmosphere. J. Geophys. Res. Atmos. 93 (D6), 7153–7168. http://dx.doi.org/10.1029/JD093iD06p07153.

Li, F., Ginoux, P., Ramaswamy, V., 2008. Distribution, transport, and deposition of mineral dust in the Southern Ocean and Antarctica: contribution of major sources. J. Geophys. Res. 113, D10207.

Lim, S., Faïn, X., Zanatta, M., Cozic, J., Jaffrezo, J.-L., Ginot, P., Laj, P., 2014. Refractory black carbon mass concentrations in snow, ice: method evaluation, intercomparison with elemental carbon measurement. Atmos. Meas. Tech. 7, 3307–3324.

Magand, O., Frezzotti, M., Pourchet, M., Stenni, B., Genoni, L., Fily, M., 2004. Climate variability along latitudinal and longitudinal transects in east Antarctica. Ann. Glaciol. 39, 351–358.

Masson-Delmotte, V., Hou, S., Ekaykin, A., Jouzel, J., Aristarain, A., Bernardo, R.T., Bromwich, D., Cattani, O., Delmotte, M., Falourd, S., Frezzotti, M., Gallée, H., Genoni, L., Isaksson, E., Landais, A., Helsen, M.M., Hoffmann, G., Lopez, J., Morgan, V., Motoyama, H., Noone, D., Oerter, H., Petit, J.R., Royer, A., Uemura, R., Schmidt, G.A., Schlosser, E., Simões, J.C., Steig, E., Stenni, B., Stievenard, M., van den Broeke, M.R., van de Wal, R.S.W., van de Berg, W.J., Vimeux, F., White, J.W.C., 2008. A review of Antarctic surface snow isotopic composition: observations, atmospheric circulation and isotopic modelling. J. Clim. 21, 3359–3387. http://dx.doi.org/10.1175/2007JCLI2139.1.

Merlivat, L., Jouzel, J., 1979. Global climatic interpretation of Deuterium-Oxygen 18 relationship for precipitation. J. Geophys. Res. 84, 5029–5033.

Millero, F.J., 1974. The physical chemistry of seawater. Annu. Rev. Earth Planet. Sci. 2, 101.

Morganti, A., Becagli, S., Castellano, E., Severi, M., Traversi, R., Udisti, R., 2007. An improved flow analysis—ion chromatography method for determination of cationic and anionic species at trace levels in Antarctic ice cores. Anal. Chim. Acta 603, 190–198.

Moteki, N., Kondo, Y., 2010. Dependence of laser-induced incandescence on physical properties of black carbon aerosols: measurements, theoretical interpretation. Aerosol Sci. Technol. 44, 663–675.

Mulvaney, R., Wagenbach, D., Wolff, E., 1998. Post depositional change in snowpack nitrate from observation of year-round near-surface snow in coastal Antarctica. J. Geophys. Res. 103, 11,021–011,031.

Palerme, C., Genthon, C., Claud, C., Kay, J.E., Wood, N.B., L'Ecuyer, T., 2016. Evaluation of current and projected Antarctic precipitation in CMIP5 models. Clim. Dyn. 1–15.

Pereira, E.B., Evangelista, H., Pereira, K.C.D., Cavalcanti, I.F.A., Setzer, A.W., 2006. Apportionment of black carbon in the South Shetland Islands, Antarctic Peninsula. J. Geophys. Res. 111, D03303. http://dx.doi.org/10.1029/2005JD006086.

Petzold, A., Ogren, J.A., Fiebig, M., Laj, P., Li, S.-M., Baltensperger, U., Holzer-Popp, T., Kinne, S., Pappalardo, G., Sugimoto, N., Wehrli, C., Wiedensohler, A., Zhang, X.-Y., 2013. Recommendations for reporting "black carbon" measurements. Atmos. Chem. Phys. 13, 8365–8379. http://dx.doi.org/10.5194/acp-13-8365-2013.

Pfahl, S., Sodemann, H., 2014. What controls deuterium excess in global precipitation? Clim. Past. Discuss. 9, 4745–4770.

Preunkert, S., Jourdain, B., Legrand, M., Udisti, R., Becagli, S., Cerri, O., 2008. Seasonality of sulfur species (dimethylsulfide, sulfate, and methanesulfonate) in Antarctica: inland versus coastal regions. J. Geophys. Res. 113, D15302. http://dx.doi.org/10.1029/2008JD009937.

Proposito, M., Frezzotti, M., 2008. Preliminary glacio-chemical analysis of GV5 and GV7 firn cores collected along the Oates Coast-Talos Dome Transect. Terra Antarct. Rep. 14, 111–116.

Rankin, A.M., Wolff, E.W., Martin, S., 2002. Frost flowers: implications for tropospheric chemistry and ice core interpretation. J. Geophys. Res. 107 (D23), 4683. http://dx.doi.org/10.1029/2002JD002492.

Sala, M., Delmonte, B., Frezzotti, M., Proposito, M., Scarchilli, C., Maggi, V., et al., 2008. Evidence of calcium carbonates in coastal (Talos Dome and Ross Sea area) East Antarctica snow and firn: environmental and climatic implications. Earth Planet. Sci. Lett. 271 (1–4), 43–52. http://dx.doi.org/10.1016/j.epsl.2008.03.045.

Scarchilli, C., Frezzotti, M., Ruti, P.M., 2011. Snow precipitation at four ice core sites in East Antarctica: provenance, seasonality and blocking factors. Clim. Dyn. http://dx.doi.org/10.1007/s00382-010-0946-4.

Schlosser, E., Oerter, H., Masson-Delmotte, V., Reijmer, C., 2008. Atmospheric

influence on the deuterium excess signal in polar firn: implications for ice-core interpretation. J. Glaciol. 54 (184), 117–124.
Schwarz, J.P., Gao, R.S., Fahey, D.W., Thomson, D.S., Watts, L.A., Wilson, J.C., Reeves, J.M., Darbeheshti, M., Baumgardner, D.G., Kok, G.L., Chung, S.H., Schulz, M., Hendricks, J., Lauer, A., Kärcher, B., Slowik, J.G., Rosenlof, K.H., Thompson, T.L., Langford, A.O., Loewenstein, M., Aikin, K.C., 2006. Single-particle measurements of midlatitude black carbon, light-scattering aerosols from the boundary layer to the lower stratosphere. J. Geophys. Res. Atmos. 111, D16.
Simmons, A., Uppala, S., Dee, D., Kobayashi, S., 2006. ERA-Interim: new ECMWF reanalysis products from 1989 onwards. ECMWF Newslett. 110, 25–35.
Spolaor, A., Vallelonga, P., Turetta, C., Maffezzoli, N., Cozzi, G., Gabrieli, J., Barbante, C., Goto-Azuma, K., Saiz-Lopez, A., Cuevas, C.A., Dahl-Jensen, D., 2016. Canadian Arctic sea ice reconstructed from bromine in the Greenland NEEM ice core. Sci. Rep. 6, 33925. http://dx.doi.org/10.1038/srep33925.
Spolaor, A., et al., 2014. Seasonality of halogen deposition in polar snow and ice. Atmos. Chem. Phys. 14, 9613–9622.
Stenni, B., Proposito, M., Gragnani, R., Flora, O., Jouzel, J., Falourd, S., et al., 2002. Eight centuries of volcanic signal and climate change at Talos Dome (East Antarctica). J. Geophys. Res. 107 (D9) http://dx.doi.org/10.1029/2000JD000317.
Stenni, B., Scarchilli, C., Masson-Delmotte, V., Schlosser, E., Ciardini, V., Dreossi, G., Grigioni, P., Bonazza, M., Cagnati, A., Frosini, D., Karlicek, D., Risi, C., Udisti, R., Valt, M., 2016. Three-year monitoring of stable isotopes of precipitation at Concordia Station, East Antarctica. Cryosphere 10, 2415.
Stephens, M., Turner, N., Sandberg, J., 2003. Particle identification by laser-induced incandescence in a solid-state laser cavity. Appl. Opt. 42, 3726–3736.
Stohl, A., Sodemann, H., 2010. Characteristics of atmospheric transport into the Antarctic troposphere. J. Geophys. Res. 115, D02305. http://dx.doi.org/10.1029/2009jd012536.
Traversi, R., Usoskin, I.G., Solanki, S.K., Becagli, S., Frezzotti, M., Severi, M., Stenni, B., Udisti, R., 2012. Nitrate in polar ice: a new tracer of solar variability. Sol. Phys. 280, 237–254. http://dx.doi.org/10.1007/s11207-012-0060-3.
Traversi, R., Udisti, R., Frosini, D., Becagli, S., Ciardini, V., Funke, B., Lanconelli, C., Petkov, B., Scarchilli, C., Severi, M., Vitale, V., 2014. Insights on nitrate sources at Dome C (East Antarctic Plateau) from multi-year aerosol and snow records. Tellus B 66, 22550. http://dx.doi.org/10.3402/tellusb.v66.22550.
Traversi, R., Becagli, S., Castellano, E., Largiuni, O., Migliori, A., Severi, M., Frezzotti, M., Udisti, R., 2004. Spatial and temporal distribution of environmental markers from coastal to plateau areas in Antarctica by firn core analysis. Intern. J. Environ. Anal. Chem. 84 (6–7), 523–536.
Udisti, R., Traversi, R., Becagli, S., Piccardi, G., 1998. Spatial distribution and seasonal pattern of biogenic sulphur compounds in snow from northern Victoria Land, Antarctica. Ann. Glaciol. 27, 535–542.
Vallelonga, P., Maffezzoli, N., Moy, A.D., Curran, M.A.J., Vance, T.R., Edwards, R., Hughes, G., Barker, E., Spreen, G., Al. Saiz-Lopez, J.P., Corella, Cuevas, C.A., Spolaor, A., 2016. Sea ice-related halogen enrichment at Law Dome, coastal East Antarctica. Clim. Past. Discuss. http://dx.doi.org/10.5194/cp-2016-74.
Watanabe, O., Kamiyama, K., Motoyama, H., Fujii, Y., Shoji, H., Satow, K., 1999. The paleoclimate record in the ice core at Dome Fuji station, East Antarctica. Ann. Glaciol. 29, 176–178.
Weller, R., Minikin, A., Petzold, A., Wagenbach, D., König-Langlo, G., 2013. Characterization of long-term and seasonal variations of black carbon (BC) concentrations at Neumayer, Antarctica. Atmos. Chem. Phys. 13, 1579–1590.
Wolff, E.W., Barbante, C., Becagli, S., Bigler, M., Boutron, C.F., Castellano, E., de Angelis, M., Federer, U., Fischer, H., Fundel, F., Hansson, M., Hutterli, M., Jonsell, U., Karlin, T., Kaufmann, P., Lambert, F., Littot, G.C., Mulvaney, R., Röthlisberger, R., Ruth, U., Severi, M., Siggaard-Andersen, M.L., Sime, L.C., Steffensen, J.P., Stocker, T.F., Traversi, R., Twarloh, B., Udisti, R., Wagenbach, D., Wegner, A., 2010. Changes in environment over the last 800 000 years from chemical analysis of the EPICA Dome C ice core. Quat. Sci. Rev. 29, 285–295.
Wolff, E.W., Cachier, H., 1998. Concentrations and seasonal cycle of black carbon in aerosol at a coastal Antarctic station. J. Geophys. Res. Atmos 103 (D9), 11033–11041.
Yang, X., Pyle, J.A., Cox, R.A., 2008. Sea salt aerosol production and bromine release: role of snow on sea ice. Geophys. Res. Lett. 35, L16815. http://dx.doi.org/10.1029/2008GL034536.